PCCP

PAPER

Excited state interactions between the chiral $Au_{38}L_{24}$ cluster and covalently attached porphyrin†

Cite this: *Phys. Chem. Chem. Phys.*, 2015, **17**, 14788

Birte Varnholt,[a] Romain Letrun,[a] Jesse J. Bergkamp,[b] Yongchun Fu,[b] Oleksandr Yushchenko,[a] Silvio Decurtins,[b] Eric Vauthey,[a] Shi-Xia Liu[b] and Thomas Bürgi*[a]

Received 20th March 2015,
Accepted 23rd April 2015

DOI: 10.1039/c5cp01638j

www.rsc.org/pccp

A protected *S*-acetylthio porphyrin was synthesized and attached to the Au_{38}(2-phenylethanethiolate)$_{24}$ cluster in a ligand exchange reaction. Chiral high performance liquid chromatography of the functionalized cluster yielded enantiomeric pairs of clusters probably differing in the binding site of the porphyrin. As proven by circular dichroism, the chirality was maintained. Exciton coupling between the cluster and the chromophore is observed. Zinc can be incorporated into the porphyrin attached to the cluster, as evidenced by absorption and fluorescence spectroscopy, however, the reaction is slow. Quenching of the chromophore fluorescence is observed, which can be explained by energy transfer from the porphyrin to the cluster. Transient absorption spectra of Au_{38}(2-phenylethanethiolate)$_{24}$ and the functionalized cluster probe the bleach of the gold cluster due to ground state absorption and the characteristic excited state absorption signals. Zinc incorporation does not have a pronounced effect on the photophysical behaviour. Decay times are typical for the molecular behaviour of small monolayer protected gold clusters.

Introduction

Systems composed of fluorophores attached to gold nanoparticles of a few nanometer in size have been widely studied for their electron transfer properties.[1,2] For understanding the mechanisms of photon capture, charge separation and charge transport, it is advantageous to work with well-defined donor–acceptor systems. Monolayer protected gold clusters are well-defined in their composition and exhibit defined optical and electronic properties. Despite the enormous interest in gold clusters over the last decade, only a handful of studies involving the incorporation of fluorophores in these well-defined systems have been reported so far.[3–7]

Porphyrins are a part of a family of macrocyclic molecules that bear large delocalized π-electron systems which give them interesting optical and electrochemical properties. Nature has utilized these properties in very elegant mechanisms such as their role in photon absorption and subsequent electron transfer pathways in photosynthesis as well as other roles in biological processes. Due to the possibility to chemically modify their structure and introduce a variety of substituents in the *meso*-position, they have found applications as building blocks for molecular electronics and artificial photosynthesis where they participate in photoinduced charge separation processes with linked donors or acceptors.[8–13]

Devadas *et al.*[3] investigated the electron transfer between the $Au_{25}(SC_6H_{13})_{18}$ cluster and modified pyrene molecules substituting some of the hexanethiolate ligands. A directional electron transfer from the cluster to the pyrene in the excited state was detected. However, no significant ground-state interactions were found. The same system was recently evaluated by Fihey *et al.*[7] in an extensive theoretical study, which confirmed that no electronic ground-state interactions take place but neither were excited state interactions calculated using a simple pyrene. These calculations predicted electron transfer from the pyrene to the cluster only if the appropriate spacer length and electron donating groups are attached to the pyrene moiety.

The wavelength dependent quenching properties of the Au_{25}(glutathione)$_{18}$ cluster with respect to non-covalently bound dyes in DNA strands were examined by Peteanu *et al.*[4] The quenching properties were found to be smaller for the Au_{25}

[a] *Department of Physical Chemistry, University of Geneva, Quai Ernest Ansermet 30, 1211 Geneva, Switzerland. E-mail: Thomas.buergi@unige.ch*
[b] *Department of Chemistry and Biochemistry, University of Bern, Freiestrasse 3, 3012 Bern, Switzerland*

† Electronic supplementary information (ESI) available: UV-vis spectra of SEC fractions, UV-vis, MALDI, and anisotropy factor spectra of HPLC fractions, CD and fluorescence spectra after Zn incorporation, TA spectra in DCM, 2D map, kinetic analysis and decay-associated difference spectra of the TA measurements. See DOI: 10.1039/c5cp01638j

cluster as compared to bigger particles, and poor quenching was observed at emission wavelengths coincident with electronic transitions.

Sakamoto *et al.*[14,15] used porphyrin derivatives with four acetylthio groups and different spacer lengths (SC_nPorph n = 0, 1 or 2) to synthesize a platonic hexahedron shaped cluster with six porphyrin molecules protecting the facets of the gold cluster containing about 66 (65) gold atoms for one (two) carbon spacer length and a cluster with 14 porphyrin molecules and 309 gold atoms for spacer length zero. A close face-on distance correlated with strong π–metal coupling was found to be responsible for broadening and a red shift of the porphyrin Soret band. Transient absorption measurements were performed for the cluster formed without spacer units. Upon excitation at 520 nm, the formation of an exciplex, followed by fast charge separation (700 fs) and recombination (32 ps) to the ground state was observed.

We herein report the functionalization of the intrinsically chiral $Au_{38}L_{24}$ cluster by a ligand exchange reaction with a porphyrin thiolate. Well-defined exchange products were isolated *via* size exclusion chromatography (SEC) and high-performance liquid chromatography (HPLC). Separation into the enantiomers allowed investigating chiral interactions by circular dichroism. A chiral orientation of the porphyrin on gold clusters combined with the incorporation of zinc is potentially interesting for chiral anion sensing. The excited state interactions between the porphyrin and the gold cluster were investigated by transient absorption (TA) spectroscopy.

Experimental

The synthesis of $Au_{38}(2PET)_{24}$ (2PET = 2-phenylethanethiolate) was performed similar to earlier reports.[16]

For the synthesis of 5-[4-(*S*-acetylthio)phenyl]-10,15,20-trismesitylporphyrin, a portion of *S*-(4-formylphenyl)ethanethiolate (0.25 g, 0.0014 mol) and 2,4,6-trimethylbenzaldehyde (1.02 g, 0.0069 mol) was dissolved in propionic acid (20 mL) and the mixture was then heated to 70 °C. At this stage, pyrrole (0.564 g, 0.0084 mol) was added to the reaction mixture and the resulting solution refluxed for 45 min. The solution was evaporated under reduced pressure and the crude mixture was passed through a pad of silica gel using dichloromethane (DCM) as an eluent. The resulting mixture was then purified by silica gel column chromatography using 60/40 DCM:hexane as an eluent to afford a purple solid. Yield 0.020 g (1.75%), ^{1}H NMR (300 MHz; $CDCl_3$): δ_H, ppm −2.53 (2H, s), 1.84 (18H, s), 2.60 (3H, s), 2.63 (9H, s), 7.28 (6H, s), 7.79 (2H, d, J = 6 Hz), 8.24 (2H, d, J = 9 Hz), 8.63 (4H, s), 8.69 (2H, d, J = 3 Hz), 8.79 (2H, d, J = 3 Hz). ESI-MS (m/z): $[M + H]^+$ calcd for $C_{55}H_{51}N_4OS$ 815.3778; found, 815.3771.

Typical reaction conditions for exchange with the porphyrin were chosen as follows: 5 mg (0.46 μmol) of $Au_{38}(2PET)_{24}$ were dissolved in tetrahydrofuran (THF). 1.5 mL of a stock solution (*ca.* 0.5 mg mL^{-1} or 0.6 μmol mL^{-1}) protected *S*-acetylthio porphyrin corresponding to *ca.* two-fold excess with respect to the cluster, 1.5 mL of aqueous ammonium hydroxide solution (10 wt%) and 1 mL of acetone were added. The components were allowed to react for 48 h at room temperature under a nitrogen atmosphere. The resulting reaction mixture was washed several times with methanol and *n*-hexane to remove salts and free porphyrin. Further purification to remove the remaining porphyrin was performed on a size exclusion column (SEC, BioRad beads S-X1, toluene, 50 cm × 1.5 cm). Moreover, the size of the unexchanged $Au_{38}(2PET)_{24}$ cluster and clusters with attached porphyrin is sufficiently different allowing preselection of the exchange products. Fractions were separated according to their UV-vis signal (Varian Cary 50 spectrometer, pathlength 2 mm, DCM). Matrix-assisted laser desorption ionization time-of-flight (MALDI-TOF) spectra were recorded on a Shimadzu Biotech Axima instrument in a positive linear mode using [3-(4-*tert*-butylphenyl)-2-methyl-2-propenylidene]-malononitrile as a matrix.

After SEC, we further separated the pre-purified fraction containing mostly single-exchanged clusters, and also unexchanged and double-exchanged clusters using a chiral HPLC column (Phenomenex Lux-Cellulose-1 column, 5 μm, 250 × 10 mm, JASCO 2070 plus UV-vis detector at 420 nm, eluent: *n*-hexane/i-propanol = 50 : 50). Five different peaks were identified and collected in several runs. It should be noted that other species are likely to be present but the chromatogram is dominated by these five superimposing peaks. The isolated fractions were analyzed by UV-vis and CD spectroscopy (JASCO J-815 spectrometer, pathlength 2 mm, DCM), MALDI-TOF mass spectrometry and by re-injection into the analytical size equivalent (250 × 4.6 mm) of the HPLC column used for the separation.

To a tetrahydrofuran/methanol (50 : 50) solution containing *ca.* 0.1 mg of $Au_{38}(2PET)_{24-n}(porphyrin)_n$ (n = 0–2) was added *ca.* five hundred-fold excess of zinc acetate which was dissolved in THF/MeOH solution. The incorporation of Zn^{2+} into the porphyrin was monitored by UV-vis spectroscopy. Additionally, zinc was incorporated into the HPLC separated fractions 4 and 5 using the above conditions and *ca.* 100-fold excess of zinc with respect to the cluster.

Steady-state fluorescence spectra were recorded on a Cary Eclipse fluorescence spectrophotometer (excitation wavelength 421 nm, excitation and emission slits 2.5 nm, 10 mm pathlength). For a comparison of fluorescence counts, the concentration of all samples was adjusted to an absorbance of 0.1 of the Soret band.

Femtosecond TA (fs-TA) measurements have been carried out using an instrument described earlier.[17,18] Excitation was performed at 400 nm using the frequency-doubled output of a Ti:sapphire amplifier (Spitfire, Spectra Physics). The pump irradiance on the sample was *ca.* 1 mJ cm^{-2}. The instrument response function (IRF) had a full width at half maximum (FWHM) of about 150 fs. The polarization of the white light probe pulses was set to a magic angle relative to that of the pump pulses.

TA measurements on a longer time scale (ns-TA) were performed using the set-up described in detail earlier.[19] Excitation at 355 nm or 532 nm was achieved with a frequency tripled

Nd:YAG laser (PowerChip, PNG-M02010-120) or a frequency-doubled Nd:YAG laser (PowerChip, PNV-M02510-120). The pump irradiance on the sample was adjusted to be similar to that used for fs-TA measurements. The FWHM of the IRF was about 350 ps. For the measurements performed at 355 nm, the probe pulses were polarized at a magic angle relative to the pump pulses, whereas they were parallel for the measurements at 532 nm excitation due to the weakness of the signal.

For both fs- and ns-TA, the samples were placed in a quartz cuvette with 1 mm pathlength and were continuously stirred by nitrogen bubbling to avoid degradation. The concentration was adjusted to an absorbance of about 0.3 at the Soret band maximum.

Results and discussion

The $Au_{38}(2PET)_{24}$ cluster structure can be described by the divide-and-protect model; it is comprised of an Au_{23} core surrounded by six SR–Au–SR–Au–SR (SR = 2-phenylethanethiolate) and three SR–Au–SR staple motifs. Ligand exchange in the staples successfully takes place with the deprotected 5-[4-thiophenyl]-10,15,20-trismesitylporphyrin. Products with up to three exchanged ligands were obtained. UV-vis spectra (Fig. S1 and S2, ESI†) show a red-shift from 419 to 421 nm and a broadening from FWHM = 11 nm to 13 nm (fitted using Origin 8.0, Voigt function) of the Soret band. The Q-bands and the absorption features of the $Au_{38}L_{24}$ cluster remain unchanged and the spectrum above 450 nm can be considered as a linear combination of porphyrin and cluster spectral components. The latter indicates that no strong ground state interaction takes place between the cluster and the fluorophore.

The porphyrin ligand has a size comparable to that of the cluster itself. Therefore, size exclusion chromatography can be used to perform a pre-purification of the product according to the number of exchanged ligands. However, no mono-dispersed fraction could be obtained.

In order to have a closer look at the prevalent species we used HPLC to separate a mixture containing mostly single exchanged, and also un-exchanged and bi-exchanged clusters (starting material). The chiral HPLC further allows separation of enantiomers from the mixture of these products. No baseline separation could be achieved on the HPLC. Chromatograms as shown in Fig. 1 display five peaks; however, due to the enantio-separation an even number of peaks are expected. Therefore we expect at least two peaks to be overlapping.

The relative intensities lead us to the assumption that P1 and P4 correspond to one enantiomeric pair and that P2 and P3 correspond to two species which can be resolved for one but not for the other enantiomer, comprising P5. Previous studies reported the racemization of different size,[20,21] ligand exchanged[22] or doped[23] clusters, making it an experiment suitable to assign the enantiomers in a chromatogram. A toluene solution of P1 and P2 was heated for 1 h at 70 °C, the chromatogram obtained after heating as displayed in Fig. 2 shows more than the two peaks expected for racemization.

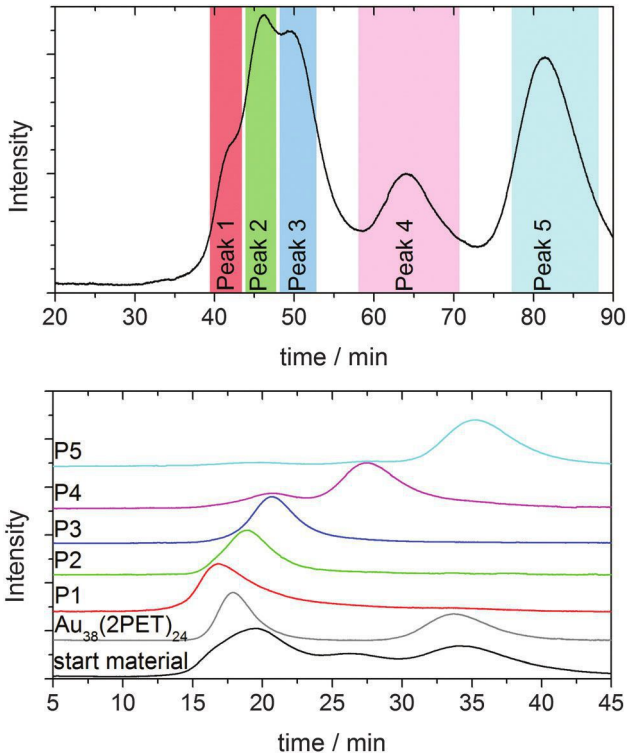

Fig. 1 HPLC chromatograms showing the starting material as used for the separation on the semi-preparative column (30 °C, 2.5 mL min^{-1}, *n*-hexane/i-propanol 1 : 1), highlighted collection intervals (top) and re-injection of a purified fraction into the analytical column (25 °C, 1.7 mL min^{-1}, *n*-hexane/i-propanol 1 : 1) and the starting solution and $Au_{38}(2PET)_{24}$ as a reference (bottom). Intensities were normalized.

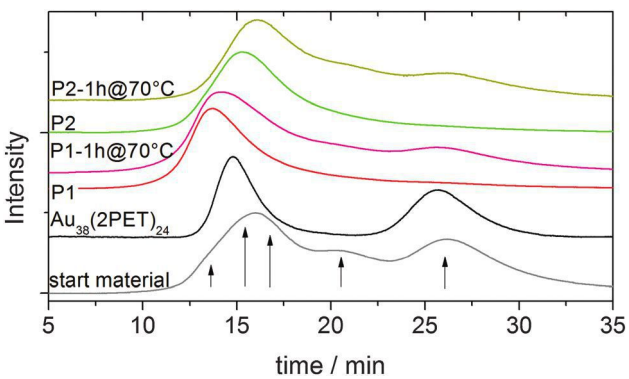

Fig. 2 HPLC chromatograms (analytical column, 30 °C, 1.7 mL min^{-1}, *n*-hexane/i-propanol 1 : 1) of fractions 1 and 2 as isolated and after heating for 1 h to 70 °C in toluene. Chromatograms of the starting material and pure $Au_{38}(2PET)_{24}$ are given as a reference. Arrows indicate retention times of the isolated fractions under these conditions. Chromatograms were normalized to the most prominent peak.

This finding indicates that not only racemization but also isomerization takes place. In the $Au_{38}L_{24}$ cluster, the thiols are bound to four symmetry unique sites. Therefore, the ligand exchange with one ligand can lead to four regio-isomers. Apparently, the porphyrin ligand can move between different symmetry unique sites, an effect earlier observed with by paracyclophane

thiol ligands on the Au38-cluster.[24] Since the kinetics of these two processes is unknown, HPLC alone is not adept for determining which peaks belong to enantiomers.

MALDI mass spectra (Fig. S3, ESI†) show a similar distribution of unexchanged, mono- and bi-exchanged clusters for all isolated peaks. As we discussed above, HPLC is not able to achieve the baseline separation, which might result in an insufficient separation of mono- and bi-exchanged products. However, a higher purity as compared to the starting material should be expected. Another possible explanation could be an intercluster exchange of ligands. We propose that this could happen when ligands desorb from one cluster and re-adsorb onto another one.[25]

The chromatographic separation of different species allows evaluating the influence of the binding position and the number of porphyrin molecules on the cluster's CD spectrum. The anisotropy factors ($g = \Delta A/A$) of the isolated fractions, with attached porphyrin, are of similar value as those of pure $Au_{38}(2PET)_{24}$ enantiomers[26] showing that the chiral structure of the cluster is maintained (Fig. S4, ESI†). Details of the shape of the anisotropy factor spectrum should not be considered since the strong absorption bands of the porphyrin necessarily provoke changes in the spectral features. For comparison, CD spectra were normalized to the ellipticity at 347 nm and are shown in Fig. 3.

While the long wavelength range (HOMO–LUMO, metal–metal transitions) stays largely unchanged, the spectra are more sensitive to the ligand shell below 500 nm.[27] Interestingly, the relative intensities of the CD bands are comparable to the pure $Au_{38}(2PET)_{24}$ spectra of P2 and P5, while for P1 and P4 the relative intensity changes. All spectra exhibit a shoulder at 420 nm, the position of the Soret band of the porphyrin ligand. This shoulder is more pronounced for P2/P5 than for P1/P4. The Soret band coincides with a zero-crossover point in the CD spectrum of the $Au_{38}(2PET)_{24}$ cluster. The appearance of this shoulder is likely due to exciton coupling between the two chromophores, porphyrin and the cluster. The use of exciton coupling between two achiral chromophores (porphyrins) attached to chiral organic molecules or achiral chromophores attached to chiral chromophores was reported earlier for chirality sensing and structure determination.[28,29] A bisignate curve is expected which is however not clear in the present spectra because of the overlaying features of the cluster itself. We postulate that the differences in the spectra might be due to different binding properties of the cluster. The amplitude of the CD signals aroused by the exciton coupling is inversely proportional to the square of the interchromophoric distance. For this reason it seems plausible to assume that the distance between porphyrin and the cluster is smaller for P2/P5 than for P1/P4; the band at 420 nm being more prominent in the spectra of the former. The reason for this could be either a different orientation of the porphyrin ligand, *e.g.* parallel or perpendicular to the cluster's long axis or attachment at different binding sites, *e.g.* outer *vs.* central sulfur atom in the long staples.

We used the separated fractions P4 and P5 to evaluate the effect of zinc incorporation on the spectra. Zinc incorporation into the macrocycle of the porphyrin increases the symmetry as compared to the free base porphyrin. Therefore, as can be seen in Fig. 4, the intensity of two degenerate Q-bands (552 and 595 nm) increases, while the other two decrease or disappear. In addition, electrons from the metal ion are donated to the

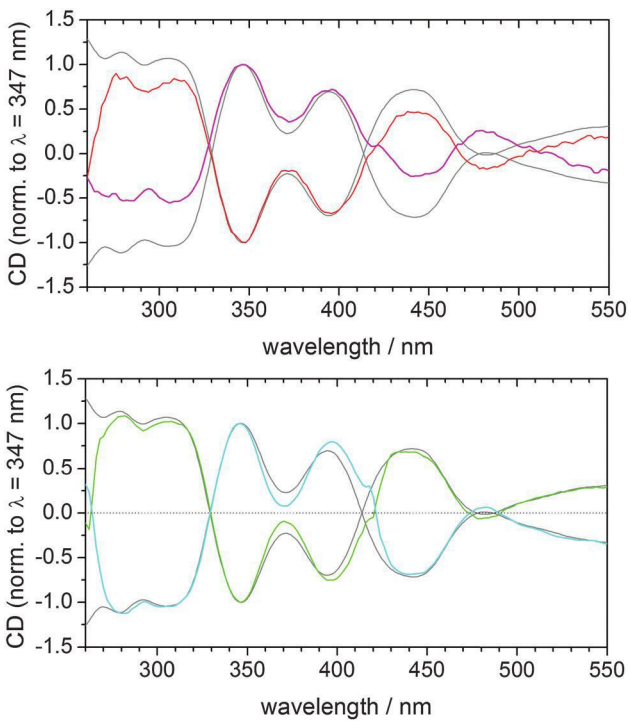

Fig. 3 CD spectra (normalized to the ellipticity at 347 nm) for the HPLC isolated fractions P1 and P4 (top) and P2 and P5 (bottom). The pairs P1, P4 and P2, P5 seem to be enantiomers. The CD spectra of the parent $Au_{38}(2PET)_{24}$ cluster is also given for comparison (grey curve).

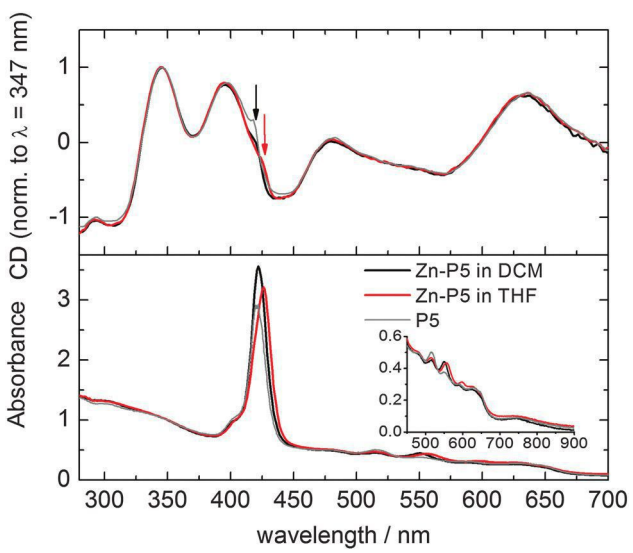

Fig. 4 CD and UV-vis spectra of the fraction P5 after Zn^{2+} incorporation measured in DCM and THF (for P4, see Fig. S5, ESI†). A red shift of the Soret band and the corresponding CD features due to coordination of THF to Zn^{2+} are observed.

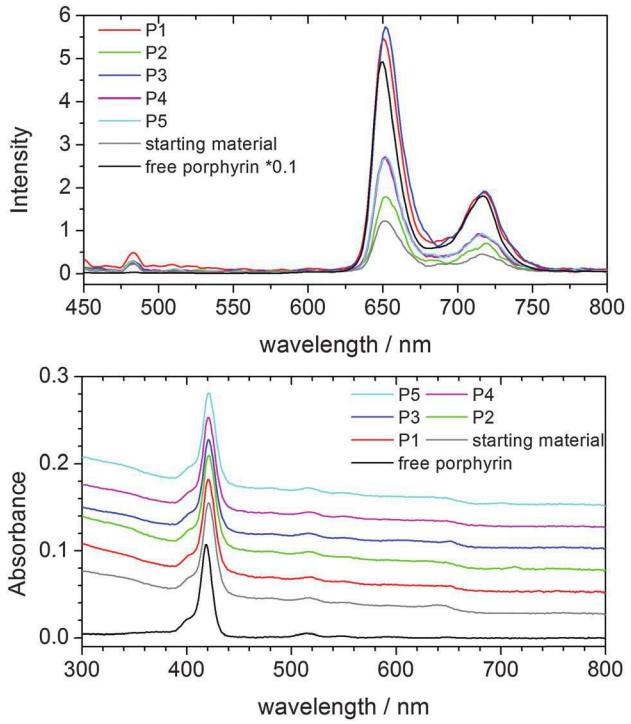

Fig. 5 Steady-state fluorescence spectra (top) and the corresponding UV-vis absorption spectra (bottom) of HPLC separated fractions.

porphyrin which lowers the transition energy.[30] A red shift of about 5 nm of both the Soret (426 nm) and Q-bands is observed. This effect is more pronounced when THF is used as a solvent instead of DCM, due to the coordination of the free electron pairs of the oxygen. Circular dichroism spectra of these samples were measured in both DCM and THF. The band due to the exciton coupling shifts with the absorption feature of the porphyrin to higher wavelengths.

Steady-state fluorescence spectra recorded in DCM upon excitation of the Soret band at 421 nm are shown in Fig. 5. The absorption spectra of the gold cluster and the porphyrin overlap additively. For the purpose of comparability of the fluorescence spectra, all spectra were normalized to the absorption difference of the peak (421 nm) and the onset (448 nm) of the Soret band.

The stationary fluorescence intensity of the porphyrin decreases by a factor of about 10 when it is attached to the cluster indicating strong excited-state interactions. These values match a previous study in which porphyrin was attached to small gold nanoparticles using a long alkyl chain linker.[31] The difference as compared to the strong quenching on bulk gold was explained by the larger distance between the porphyrin and the nanoparticles, and the strong curvature of the nanoparticles. In our case, only a phenylthiolate separates the porphyrin macrocylce from the gold cluster and hence the distance between the two is very small.

Quenching efficiency depends not only on the distance but also on the orientation, which might explain the observed differences between the five HPLC collected fractions. However, we assume from CD data and HPLC chromatograms that P1/P4 and P2/P5 are enantiomers; P3 was not assigned. Thus, we expect the quenching efficiency of these pairs of enantiomers to be the same. Comparing MALDI spectra with the quenching efficiency, it appears that the fractions containing the highest relative amount of bi-exchanged clusters (P1 and P3) are less quenched than those with relatively lower amounts of bi-exchanged clusters (P2, P4, and P5). It may be assumed that bi-exchanged clusters have shorter retention times on the HPLC and elute preferentially with P1 (possibly corresponding to bi-exchanged enantiomer 1) and P3 (possibly corresponding to bi-exchanged enantiomer 2). Despite the small amounts even in P1 and P3, the effect is quite prominent. When two fluorophores are attached to one cluster, the probability for quenching decreases as compared to one fluorophore per cluster. Zinc incorporation leads to the expected blue shift of the fluorescence signals (Fig. S6, ESI†).[30] However, the signals of the free-base porphyrin attached to the cluster are still observed as well. Despite the large excess of Zn^{2+} during the incorporation reaction, free-base and the metalloporphyrin are present in the samples. The reaction with the separated samples was stopped after 24 h to prevent racemization of the cluster which has been shown to take place in solution.[20] Additionally, a sample of the starting material used for the separation was allowed to react with a zinc acetate solution over one week. The spectrum shows only the characteristic signals of the metalloporphyrin. The kinetics of the zinc incorporation is slow, presumably due to a steric hindrance, *i.e.* Zn^{2+} ions cannot easily reach the porphyrin ring due to shielding by other ligands of the shell.

Transient absorption (TA) measurements were performed with the individual building blocks (porphyrin and the $Au_{38}(2PET)_{24}$ cluster) as well as with the functionalized cluster to obtain a deeper insight into the quenching mechanism, which can be due to electron or energy transfer. Measurements were done for the HPLC purified samples, but since these were not obtained in a mono-dispersed form, reference measurements were performed on the starting material (before HPLC) to evaluate the influence of the purity of the samples. Note that all samples, independent of mono-dispersity, show the same behavior. Neither the number (if low enough) nor the position of the ligand seems to have an impact. As expected, the fs-TA spectra of the free-base porphyrin recorded upon 400 nm excitation show essentially no evolution over the whole temporal window of the experiment (Fig. 6). The negative signals at about 420 and 515 nm corresponding to the ground state bleach (GSB) of the Soret and Q bands, respectively, are separated by a weak excited state absorption (ESA).

On the other hand, the TA spectra of the cluster recorded upon 400 nm (fs-TA) and 355 nm (ns-TA) excitation contain more features that cover the entire spectral window of the experiment (Fig. 6 and Fig. S7, ESI†). They are characterized by two negative signals between 420 and 500 nm and at around 640 nm that can be assigned to the GSB by comparison with the stationary absorption spectrum. Additionally, two positive signals are observed, a broad one extending from 500 to 620 nm and another weaker one above 670 nm. These are assigned to the ESA of the gold cluster, and are similar to earlier reports.[32–34]

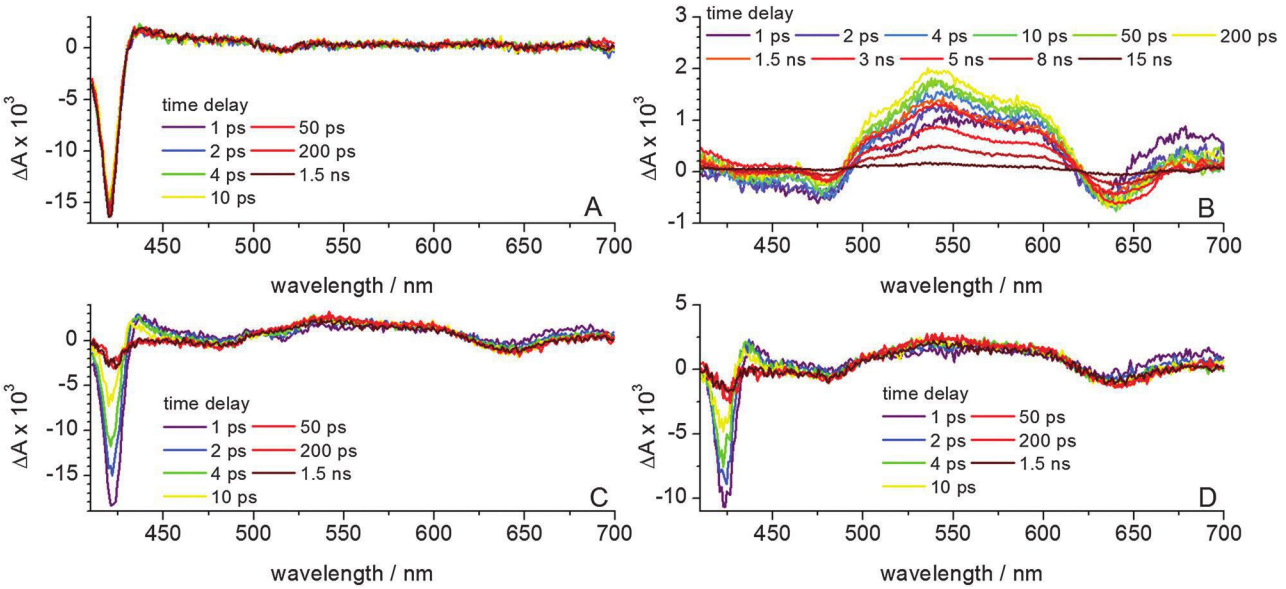

Fig. 6 Transient absorption spectra of (A) free-base porphyrin, (B) $Au_{38}(2PET)_{24}$, (C) $Au_{38}(2PET)_{24-n}(porphyrin)_n$ (n = 0–2) and (D) $Au_{38}(2PET)_{24-n}(Zn\text{-}porphyrin)_n$ (n = 0–2) in toluene. Spectra from 1 ps to 1.5 ns were recorded after excitation at 400 nm while for the spectra 3 ns to 15 ns an excitation wavelength 355 nm was used.

An initial rise of the signal, mostly visible in the central ESA, with a time constant of 3.2 ps in toluene (6.5 ps in DCM) is observed and is assigned to a thermalization effect.[35,36] The steady-state absorption spectrum of the Au_{38} cluster is known to be temperature dependent.[37] Irradiation at 400 nm locally heats the cluster and thus excites vibrations of the core gold atoms as well as the staples which influence the electronic structure. The 2D plot (Fig. S8, ESI†) below 500 nm reveals periodic oscillations of the TA signal intensity due to a vibrational wavepacket at 283 cm^{-1} probably belonging to the shell breathing mode.[35,38] After vibrational relaxation, the decay of the excited-state population takes place with a time constant of 5.3 ns, independently of the solvent. Overall, a similar behavior is observed in toluene (TOL) and dichloromethane (DCM) for both the porphyrin and the cluster.

The fs-TA measurements with the functionalized cluster were performed upon 400 nm excitation resulting in unavoidable direct excitation of the gold cluster additionally to the excitation of porphyrin. The spectra therefore contain a combination of the features observed previously with two individual components. Nevertheless, a striking difference in the dynamics of the GSB of porphyrin's Soret band can be observed. The bleach decreases by more than 80% within the first 50 ps and then remains constant up to 1.5 ns (Fig. S9, ESI†). This process is accompanied by a blue shift of the positive signal located at the red edge of the GSB on a similar time scale. Such a behavior is typical for the cooling of the vibrationally hot electronic ground state.[39,40]

The facts that the Soret band bleach recovers and that the dynamics is essentially identical in non-polar and polar solvents strongly disfavor electron transfer as the quenching mechanism. If charge separation was to take place, the very fast bleach recovery could only be explained by a charge recombination faster than the separation. Furthermore, the absorption spectrum of the zinc porphyrin radical cation is known to have its most intense band at 410 nm.[41] This feature, previously observed by TA in systems where electron transfer takes place,[42] is absent here. The lack of this spectral feature also goes against the occurrence of charge separation, at least from the porphyrin to the cluster. For all these reasons, the quenching observed here is attributed to energy transfer that is frequent with functionalized gold clusters.[1]

Table 1 Time constants obtained from the global analysis of the TA spectra shown in Fig. 6

Compound	Solvent	τ_1/ps	τ_2/ps	τ_3/ns
Porph-cluster	TOL	1.5	10	>2
	DCM	1.8	17	>2
Zn-Porph-cluster	TOL	1.0	12	>2
	DCM	1.2	15	>2

A global analysis of the spectra yielded three time constants that are collected in Table 1. The decay-associated difference spectrum of the shortest component, τ_1, contains a major contribution from the Soret band GSB, whereas the spectrum associated with τ_2 exhibits features of the GSB and ESA (Fig. S10, ESI†). Therefore, τ_1 is ascribed to energy transfer from the excited porphyrin to the cluster and τ_2 to subsequent vibrational relaxation of the hot ground state. The spectrum associated with the longest time constant, τ_3, is mainly due to the directly excited clusters, but also contains some residual Soret band bleach. This bleach, which slowly recovers on a μs time scale (Fig. S9, ESI,† inset), could be due to porphyrins in the triplet state that are not quenched because of an unfavorable orientation for energy transfer, or could indicate that electron transfer may after all be a parallel quenching mechanism, despite the data providing no clear evidence to support this hypothesis.

The incorporation of zinc into the macrocycle does not change the behavior. The shape and the dynamics of the TA spectra are comparable to the above discussed compounds. This can be seen as another proof for energy transfer of the quenching mechanism since the incorporation of zinc lowers the oxidation and reduction potentials of the porphyrin by about 0.2 eV.[43]

Conclusion

Functionalization of the well-defined chiral $Au_{38}L_{24}$ cluster with on average one porphyrin ligand leads to different isomers, which can be separated by HPLC. The chirality of the cluster is maintained and the exciton coupling between the two chromophores, porphyrin and the cluster, is observed. The strength of the exciton coupling allows differentiation of isomers. Steady state absorption spectra of the functionalized cluster are the sum of the individual components indicating that ground state interactions are not important. The incorporation of zinc into the porphyrin ring does not change this. However, excited state interactions take place as proven by fluorescence quenching and transient absorption measurements. The TA decay of the Soret bleach indicates energy transfer from the porphyrin to the gold cluster. Furthermore, the TA spectrum of the cluster itself shows independently of the shell composition GSB and ESA signals. The GSB reveals molecular vibrations of the cluster, likely corresponding to the breathing modes.

Acknowledgements

Financial support from the Swiss National Science Foundation (project numbers 200020-152596 and 200021-147143), the University of Geneva and the University of Bern is kindly acknowledged. We are grateful to Sandra Mosquera-Vázquez for her help in the ns-TA measurements. We thank Sophie Michalet for MALDI measurements.

Notes and references

1 K. G. Thomas and P. V. Kamat, *Acc. Chem. Res.*, 2003, **36**, 888–898.
2 D. M. Adams, L. Brus, C. E. D. Chidsey, S. Creager, C. Creutz, C. R. Kagan, P. V. Kamat, M. Lieberman, S. Lindsay, R. a. Marcus, R. M. Metzger, M. E. Michel-Beyerle, J. R. Miller, M. D. Newton, D. R. Rolison, O. Sankey, K. S. Schanze, J. Yardley and X. Zhu, *J. Phys. Chem. B*, 2003, **107**, 6668–6697.
3 M. S. Devadas, K. Kwak, J.-W. Park, J.-H. Choi, C.-H. Jun, E. Sinn, G. Ramakrishna and D. Lee, *J. Phys. Chem. Lett.*, 2010, **1**, 1497–1503.
4 S. Chowdhury, Z. Wu, A. Jaquins-Gerstl, S. Liu, A. Dembska, B. A. Armitage, R. Jin and L. A. Peteanu, *J. Phys. Chem. C*, 2011, **115**, 20105–20112.
5 Y. Negishi, U. Kamimura, M. Ide and M. Hirayama, *Nanoscale*, 2012, **4**, 4263–4268.
6 B. B. Narakathu, M. S. Devadas, A. S. G. Reddy, A. Eshkeiti, A. Moorthi, I. R. Fernando, B. P. Miller, G. Ramakrishna, E. Sinn, M. Joyce, M. Rebros, E. Rebrosova, G. Mezei and M. Z. Atashbar, *Sens. Actuators, B*, 2013, **176**, 768–774.
7 A. Fihey, F. Maurel and A. Perrier, *J. Phys. Chem. C*, 2014, **118**, 4444–4453.
8 T. A. Moore, D. Gust, P. Mathis, J.-C. Mialocq, C. Chachaty, R. V. Bensasson, E. J. Land, D. Doizi, P. A. Liddell, W. R. Lehman, G. A. Nemeth and A. L. Moore, *Nature*, 1984, **307**, 630–632.
9 D. Holten, D. F. Bocian and J. S. Lindsey, *Acc. Chem. Res.*, 2002, **35**, 57–69.
10 D. Gust, T. A. Moore and A. L. Moore, *Acc. Chem. Res.*, 2009, **42**, 1890–1898.
11 M. R. Wasielewski, *Acc. Chem. Res.*, 2009, **42**, 1910–1921.
12 H. Jia, B. Schmid, S. X. Liu, M. Jaggi, P. Monbaron, S. V. Bhosale, S. Rivadehi, S. J. Langford, L. Sanguinet, E. Levillain, M. E. El-Khouly, Y. Morita, S. Fukuzumi and S. Decurtins, *ChemPhysChem*, 2012, **13**, 3370–3382.
13 D. Villamaina, M. M. A. Kelson, S. V. Bhosale and E. Vauthey, *Phys. Chem. Chem. Phys.*, 2014, **16**, 5188–5200.
14 M. Sakamoto, D. Tanaka, H. Tsunoyama, T. Tsukuda, Y. Minagawa, Y. Majima and T. Teranishi, *J. Am. Chem. Soc.*, 2012, **134**, 816–819.
15 D. Tanaka, Y. Inuta, M. Sakamoto, A. Furube, M. Haruta, Y.-G. So, K. Kimoto, I. Hamada and T. Teranishi, *Chem. Sci.*, 2014, **5**, 2007–2010.
16 H. Qian, Y. Zhu and R. Jin, *ACS Nano*, 2009, **3**, 3795–3803.
17 G. Duvanel, N. Banerji and E. Vauthey, *J. Phys. Chem. A*, 2007, **111**, 5361–5369.
18 N. Banerji, G. Duvanel, A. Perez-Velasco, S. Maity, N. Sakai, S. Matile and E. Vauthey, *J. Phys. Chem. A*, 2009, **113**, 8202–8212.
19 B. Lang, S. Mosquera-Vázquez, D. Lovy, P. Sherin, V. Markovic and E. Vauthey, *Rev. Sci. Instrum.*, 2013, **84**, 073107.
20 S. Knoppe, I. Dolamic and T. Bürgi, *J. Am. Chem. Soc.*, 2012, **134**, 13114–13120.
21 B. Varnholt, I. Dolamic, S. Knoppe and T. Bürgi, *Nanoscale*, 2013, **5**, 9568–9571.
22 S. Knoppe, S. Michalet and T. Bürgi, *J. Phys. Chem. C*, 2013, **117**, 15354–15361.
23 N. Barrabés, B. Zhang and T. Bürgi, *J. Am. Chem. Soc.*, 2014, **36**, 4–7.
24 L. Beqa, D. Deschamps, S. Perrio, A.-C. Gaumont, S. Knoppe and T. Bürgi, *J. Phys. Chem. C*, 2013, **117**, 21619–21625.
25 Y. Niihori, W. Kurashige, M. Matsuzaki and Y. Negishi, *Nanoscale*, 2013, **25**, 508–512.
26 I. Dolamic, S. Knoppe, A. Dass and T. Bürgi, *Nat. Commun.*, 2012, **3**, 798–804.
27 O. Lopez-Acevedo, H. Tsunoyama, T. Tsukuda, H. Häkkinen and C. M. Aikens, *J. Am. Chem. Soc.*, 2010, **132**, 8210–8218.
28 S. Matile and N. Berova, *J. Am. Chem. Soc.*, 1996, **7863**, 5198–5206.
29 W. T. Wiesler, N. Berova, M. Ojika, H. V. Meyers, M. Chang, P. Zhou, L.-C. Lo, M. Niwa, R. Takeda and K. Nakanishi, *Helv. Chim. Acta*, 1990, **73**, 509–551.
30 W. Zheng, N. Shan, L. Yu and X. Wang, *Dyes Pigm.*, 2008, **77**, 153–157.

31 H. Imahori, M. Arimura, T. Hanada, Y. Nishimura, I. Yamazaki, Y. Sakata and S. Fukuzumi, *J. Am. Chem. Soc.*, 2001, **123**, 335–336.
32 S. Link, M. A. El-Sayed, T. G. Schaaff and R. L. Whetten, *Chem. Phys. Lett.*, 2002, **356**, 240–246.
33 S. A. Miller, J. M. Womick, J. F. Parker, R. W. Murray and A. M. Moran, *J. Phys. Chem. C*, 2009, **113**, 9440–9444.
34 S. H. Yau, O. Varnavski, J. D. Gilbertson, B. Chandler, G. Ramakrishna and T. Goodson, *J. Phys. Chem. C*, 2010, **114**, 15979–15985.
35 S. H. Yau, O. Varnavski and T. Goodson, *Acc. Chem. Res.*, 2013, **46**, 1506–1516.
36 S. Mustalahti, P. Myllyperkiö, S. Malola, T. Lahtinen, K. Salorinne, J. Koivisto, H. Häkkinen and M. Pettersson, *ACS Nano*, 2015, **9**, 2328–2335.
37 M. S. Devadas, S. Bairu, H. Qian, E. Sinn, R. Jin and G. Ramakrishna, *J. Phys. Chem. Lett.*, 2011, **2**, 2752–2758.
38 B. Varnholt, P. Oulevey, S. Luber, C. Kumara, A. Dass and T. Bürgi, *J. Phys. Chem. C*, 2014, **118**, 9604–9611.
39 J. Grilj, P. Buchgraber and E. Vauthey, *J. Phys. Chem. A*, 2012, **116**, 7516–7522.
40 J. Grilj, C. Zonca, L. M. L. Daku and E. Vauthey, *Phys. Chem. Chem. Phys.*, 2012, **14**, 6352–6358.
41 A. N. Okhrimenko, A. V. Gusev and M. A. J. Rodgers, *J. Phys. Chem. A*, 2005, **109**, 7653–7656.
42 D. Villamaina, S. V. Bhosale, S. J. Langford and E. Vauthey, *Phys. Chem. Chem. Phys.*, 2013, **15**, 1177–1187.
43 A. Giraudeau, H. J. Callot and M. Gross, *Inorg. Chem.*, 1979, **18**, 201–206.